

Understanding the 1P- and 2S nucleon resonances within the extended Lee-Friedrichs Model

Yu-Hui Zhou,¹ Hui-Hua Zhong,² Zhi-Yong Zhou,^{1,*} and Xian-Hui Zhong^{3,4,†}

¹*School of Physics, Southeast University, Nanjing 211189, P. R. China*

²*College of Aeronautics Mechanical and Electrical Engineering, Jiangxi Flight University, Nanchang 330088, China*

³*Department of Physics, Hunan Normal University, and Key Laboratory of Low-Dimensional Quantum Structures and Quantum Control of Ministry of Education, Changsha 410081, China*

⁴*Synergetic Innovation Center for Quantum Effects and Applications (SICQEA), Hunan Normal University, Changsha 410081, China*

(Dated: April 23, 2026)

We present a unified description of the low-lying 1P and 2S-wave nucleon resonance within the framework of an extended Lee-Friedrichs scheme. By incorporating the coupled-channel dynamics between bare quark-model states and the πN , $\pi\Delta$ and ηN meson-baryon continua, we examine the mass shifts and structural properties of these excited states. We demonstrate that when the model parameters are calibrated to match the 1P-wave spectrum and their widths, the pole associated with the bare 2S state is naturally shifted downward to the mass region of physical Roper resonance- $N(1440)$, thereby offering a dynamical explanation for the long-standing level-inversion problem. An approximate analysis of compositeness and elementariness reveals that the Roper resonance contains a significant meson-baryon continuum states, consistent with the picture of a bare core heavily dressed by meson-baryon cloud. Simultaneously, the pole positions and properties of five 1P-wave resonances- $N(1535)$, $N(1650)$, $N(1520)$, $N(1700)$ and $N(1675)$ are successfully reproduced. Our results highlight the essential role of coupled-channel effects in shaping the nucleon spectrum and provide a consistent microscopic insight into the interplay between internal quark degrees of freedom and external hadronic fields.

I. INTRODUCTION

Understanding the spectroscopy of excited baryon resonances is crucial for elucidating the non-perturbative dynamics of Quantum Chromodynamics (QCD) in the confinement regime. In recent decades, high-precision photoproduction and electroproduction experiments at facilities such as JLab, MAMI, ELSA, BES III and Belle II have amassed a wealth of data, significantly enriching the baryon spectrum. However, extracting reliable resonance parameters from these data remains a formidable challenge. Similar to the meson sector or even worse, the baryon resonances are usually broad and overlapping with each other, which makes the identification of their internal structure and properties highly sensitive to the theoretical ansatz employed in the Partial Wave Analysis (PWA). Among these elusive states, the Roper resonance- $N(1440)$, with spin-parity quantum number $J^P = 1/2^+$ [1], stands out as one of the most enigmatic puzzles.

The primary theoretical difficulty concerning the Roper resonance is the well-known mass inversion problem. In the conventional quark model based on the one-gluon-exchange (OGE) and confinement interactions, usually the first orbital excited states ($N=1$, $L=1$) are expected to lie significantly lower in mass than the first radial excited states ($N=2$, $L=0$). Indeed, the conventional quark model has been remarkably successful in describing the “normal” sector of the baryon spectrum; the five experimentally established 1P-wave nucleon resonances, such as $N(1535)1/2^-$, $N(1520)3/2^-$, $N(1650)1/2^-$, $N(1700)3/2^-$ and $N(1675)5/2^-$, follow the mass ordering predicted by three-quark dynamics reasonably well. However, $N(1440)$ appears roughly 100 MeV below the

$N(1535)$. This observation implies that the first radial excitation is lighter than the first orbital excitation, a level ordering that directly contradicts the expectations of potential models. Consequently, the nature of the $N(1440)$ has been investigated extensively across various frameworks, including lattice QCD, Faddeev equations and effective field theory [2–15].

Motivated by this discrepancy, subsequent efforts have been devoted to refine the consistent quark model formulation. The relativized quark model developed in Refs. [16, 17] claimed the problem was tamed when relativistic kinematics are incorporated, yet these improvements did not change the ordering of the energy levels. By introducing the one-boson-exchange (OBE) hyperfine interaction [18], the mass inversion between the Roper resonance and the $N(1535)$ can be reproduced. Unlike the flavor-blind confinement potential, the spin-flavor dependence of the OBE interaction provides additional attraction for the spatially symmetric wave function of the Roper resonance, thereby lowering its mass below that of the $N(1535)$. Furthermore, in hybrid quark models incorporating both OGE and OBE potentials, it was found that the mass of $N(2S, 1/2^+)$ is lowered about 400 MeV, whereas the 1P-wave nucleons are only shifted by only roughly 100 MeV [19]. Similar conclusions emerge from unquenched quark models [20], where the screening effects of quark-antiquark pairs are considered. These results collectively suggest that the Roper resonance cannot be viewed as a pure three-quark state but new mechanisms should be adopted to understand its nature.

Beyond the mass spectrum, the exceptionally large width of the Roper resonance also poses a severe challenge for physical interpretation [21–26]. The commonly used Breit-Wigner formalism, while adequate for narrow states, becomes unreliable for such broad resonances since the threshold effects and unitarity constraints usually play an important role in correctly understanding their information. Rigorously, a resonance is defined as a pole of the S -matrix on the un-physical Riemann sheet of complex energy plane. To understand the dynamical

*zhouzhy@seu.edu.cn

†zhongxh@hunnu.edu.cn

origin of these broad resonances, it is necessary to consider the coupled-channel effects and study the properties by analytically continuing into the complex energy plane.

To date, several studies utilizing the dynamical coupled-channel models have made progress in extracting the Roper pole from πN and $\pi\pi N$ scattering data, providing valuable insights into multi-channel resonance dynamics [2, 23, 27–32]. Suzuki et al. [2] claimed that $N(1440)$ and $N(1710)$ evolve from a single bare nucleon state with a mass of 1.763 GeV by tracing pole trajectories as the couplings were turned on. In a different approach, Wang et al. [32] demonstrated that $N(1440)$ can also be generated purely dynamically through t - and u -channel hadron-exchange dynamics, without introducing any s -channel bare state. Their result is consistent with early results of a coupled-channel meson-exchange model [33]. These varying interpretations highlight the need for a theoretical framework that can transparently disentangle the contributions of intrinsic quark core from the dynamical dressing of the meson cloud.

Along these lines, we employ the extended Lee-Friedrichs (LF) scheme [34–37]. This formalism offers a rigorous solvable Hamiltonian framework that allows for an exact treatment of the coupling between discrete bare states and continuum channels, fully preserving unitarity and analyticity. The exact solvability provides a clear and transparent way to disentangle the contributions of bare discrete state and coupled continuum states, which could be applied into the baryon systems to study the intrinsic quark-core and coupled channels. Furthermore, embedding this scheme into the rigged Hilbert space (RHS) providing a solid mathematical foundation for understanding the complex eigenvalue of Hamiltonian, their wave functions, and other related properties [38]. Consequently, this approach offers a complementary perspective on the formation and properties of the resonance, linking underlying quark dynamics directly to observable features such as pole positions and widths.

In this work, we extend the LF model combined with the quark pair creation (QPC) model to the nucleon system for the first time, aiming to clarify the dynamical origin and structure of the Roper resonance and other orbital excited state through a consistent coupled channel analysis.

This paper is organized as follows. The theoretical foundations are introduced in Sec. II, which include the Lee-Friedrichs model, the potential model and the QPC model. The numerical calculations and analysis are given in Sec. III. Sec. IV contains our final conclusion and summary.

II. THEORETICAL FRAMEWORK

A. The extended Lee-Friedrichs scheme

The Lee-Friedrichs model describes how resonance phenomena occur when a discrete bare state couples to a continuum state [39, 40]. When extended to a more general version with multiple continuum states and with multiple discrete states, the model remains to be exactly solvable and satisfies the unitarity of the S -matrix so that it has a more general phe-

nomenological application in hadron physics [34–37]. When we consider a discrete bare state coupled with multiple continuum states (or called scattering channels), the total Hamiltonian is given by $H = H_0 + V$, where H_0 represents the free Hamiltonian and V the interaction term. The free Hamiltonian is expressed as

$$H_0 = m_0|1\rangle\langle 1| + \sum_i \int_{\omega_{\text{th},i}}^{\infty} E|E, i\rangle\langle E, i|dE, \quad (1)$$

where $|1\rangle$ and $|E, i\rangle$ denote the discrete state and the i -th continuum state, respectively. The normalization conditions for the bare states are

$$\begin{aligned} \langle 1|1\rangle &= 1, \quad \langle 1|E, i\rangle = \langle E, i|1\rangle = 0, \\ \langle E, i|E', j\rangle &= \delta_{ij}\delta(E - E'). \end{aligned} \quad (2)$$

The index i labels the quantum numbers of a given continuum state, including the particle species, total spin S and orbital angular momentum L . We denote the bare mass of the discrete state by m_0 while $\omega_{\text{th},i}$ represents the energy threshold of the i -th continuum state. The interaction term is expressed as

$$V = \sum_i \int_{\omega_{\text{th},i}}^{\infty} (f_i(E, i)|E, i\rangle\langle 1| + f_i^*(E)|1\rangle\langle E, i|)dE, \quad (3)$$

where the coupling between $|1\rangle$ and $|E, i\rangle$ is characterized by a vertex function $f_i(E)$. The conservation of the total angular momentum and its third component is implicit. Solving the eigenvalue problem

$$H|\Psi(x)\rangle = x|\Psi(x)\rangle, \quad (4)$$

within the RHS provide a solid mathematical foundation for studying resonance phenomenon in the coupled system. Because of the completeness relation

$$|1\rangle\langle 1| + \sum_i \int_{\omega_{\text{th},i}}^{\infty} |E, i\rangle\langle E, i|dE = 1, \quad (5)$$

the general solution of wave function $\Psi(x)$ is supposed to be expanded in the basis of discrete and continuum states as

$$|\Psi(x)\rangle = \alpha(x)|1\rangle + \sum_i \int_{\omega_{\text{th},i}}^{\infty} \psi_i(x, E)|E, i\rangle dE, \quad (6)$$

where $\alpha(x)$ is a complex function and $\psi_i(x, E)$ represents a distribution over the continuum states. By substituting the general solution to the eigenfunction and projecting it on the bases, the solutions could be written down as

$$\begin{aligned} |\Psi_0(x)\rangle &= \alpha(x) \left[|1\rangle + \sum_i \int_{\omega_{\text{th},i}}^{\infty} \frac{f_i(E)}{x - E + i\epsilon} |E, i\rangle dE \right], \quad (x < \omega_{\text{th},1}) \\ |\Psi_i^\pm(x)\rangle &= |x\rangle_i + \frac{f_i^*(x)}{\eta^\pm(x)} \left[|1\rangle + \sum_i \int_{\omega_{\text{th},i}}^{\infty} \frac{f_i(E)}{x - E + i\epsilon} |E, i\rangle dE \right], \\ &\quad (\omega_{\text{th},i} < x < \omega_{\text{th},i+1}) \end{aligned} \quad (7)$$

where $i\epsilon$ in the denominator is introduced for avoiding the singularity at $x = E$. From the prospective of scattering theory, $|\Psi_i^+(x)\rangle$ is the “in” state and $|\Psi_i^-(x)\rangle$ is the “out” state.

The scattering S matrix is obtained by the inner product of the “in” and “out” state, and the unstable intermediate state is represented by the pole of the scattering amplitude. The key ingredient in solving the eigenvalue problem of Eq. (4), determining the resonance eigenvalues and constructing the wave functions within the RHS is the inverse resolvent function $\eta(x)$, expressed as

$$\eta(x)^\pm = x - m_0 - \sum_i \int_{\omega_{\text{th},i}}^{\infty} \frac{|f_i(E)|^2}{x - E \pm i\epsilon} dE. \quad (8)$$

The $\eta(x)^\pm$ function has cuts starting from every energy threshold $\omega_{\text{th},i}$ to the infinity. After analytical continuation to different Riemann sheets (RS) on the complex energy plane, the resonance poles are represented by $\eta(z) = 0$. Bound state poles are located below the first threshold on the first RS while resonances are located on the other RSs. The resonance pole is defined as

$$z_R = M - \frac{i}{2}\Gamma, \quad (9)$$

where M and Γ are the mass and width of the resonance pole, respectively.

For multi-channel case, each threshold $\omega_{\text{th},i}$ introduces a branch cut, resulting in a total of 2^n Riemann sheets. In this paper, we are going to deal with the situation with three channels,

$$\eta^{\text{II}}(z) = \eta^{\text{I}}(z) - 2\pi i G_1(z), \quad (10)$$

$$\eta^{\text{III}}(z) = \eta^{\text{I}}(z) - 2\pi i G_1(z) - 2\pi i G_2(z), \quad (11)$$

$$\eta^{\text{IV}}(z) = \eta^{\text{I}}(z) - 2\pi i G_1(z) - 2\pi i G_2(z) - 2\pi i G_3(z), \quad (12)$$

in which $G_i(z) = f_i(z)f_i^*(z)$ represents the analytical continuation of the module square of the coupling function of the i -th channel and I, II, III and IV label the first, second, third and fourth sheets, respectively. Here, we only focus on the un-physical Riemann sheets which is closest to the physical sheet, since the poles on these sheets are close to the physical region.

The wave function of a bound state with real eigenvalue z_B can be explicitly represented as

$$|z_B\rangle = N_B \left(|1\rangle + \sum_i \int_{\omega_{\text{th},i}}^{\infty} \frac{f_i(E)}{z_B - E} dE |E, i\rangle \right), \quad (13)$$

with the normalization defined as $\langle z_B | z_B \rangle = 1$, and

$$N_B = \left(1 + \sum_i \int_{\omega_{\text{th},i}}^{\infty} \frac{|f_i(E)|^2}{(z_B - E)^2} dE \right)^{-1/2}. \quad (14)$$

The wave function of a resonance with complex eigenvalue z_R can be explicitly represented as

$$|z_R\rangle = N_R \left(|1\rangle + \sum_i \int_{\omega_{\text{th},i}}^{\infty} \frac{f_i(E)}{[z_R - E]_+} dE |E, i\rangle \right),$$

$$\langle \bar{z}_R | = N_R \left(\langle 1 | + \sum_i \int_{\omega_{\text{th},i}}^{\infty} \frac{f_i(E)}{[z_R - E]_+} dE \langle E, i | \right).$$

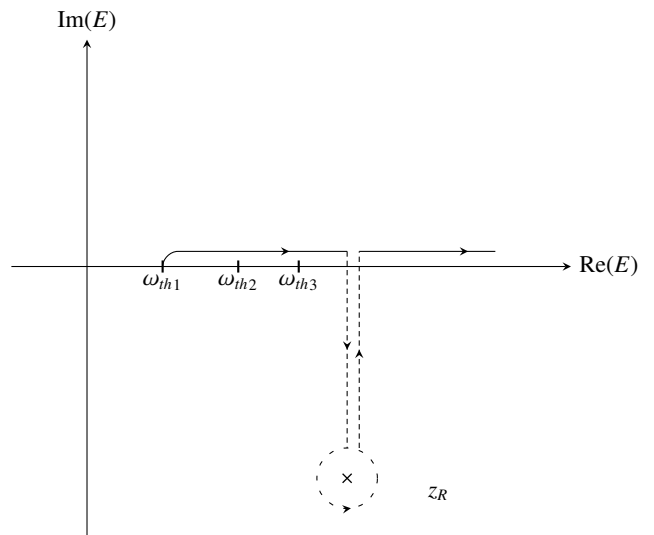


FIG. 1: The deformation of the integral path. The dashed line means the path on the RS where the pole is located.

It is worth emphasizing that the subscript “+” denotes the integration contour which begins at the threshold along the upper rim of the branch cut and it has to be deformed to encircle the resonance pole in a counter-clockwise direction when it passes the physical region where the RS of resonance pole is attached, as shown in Fig. 1 [36]. The normalization factor N_R is given by

$$N_R = \left(1 + \sum_i \int_{\omega_{\text{th},i}}^{\infty} \frac{|f_i(E)|^2}{[z_R - E]_+^2} dE \right)^{-1/2}, \quad (15)$$

where the integration contour is similarly defined as mentioned above. The normalization is usually defined as $\langle \bar{z}_R | z_R \rangle = 1$, since the usually normalization gives $\langle z_R | z_R \rangle = 0$.

B. The Potential Model

1. Hamiltonian

In this framework, the bare mass m_0 and the wave function of a nucleon in Eq. (8) are described by the potential model. This treatment is justified as an effective description at low energy regions, where the baryon dynamics are well captured by constituent quarks interacting through phenomenological potentials. While the non-relativistic quark model (NRQM) involves certain simplifications, it has proven successful in describing the light-baryon spectrum, reproducing the SU(3) octet–decuplet structure, hyperfine splittings, and mass systematics across the light-baryon families [41–44]. Consequently, it provides a reasonable and widely adopted basis for specifying the bare mass of low-lying excited nucleons in the coupled-channel analysis. Accordingly, we utilize the NRQM to calculate the bare masses and adopt a Hamiltonian of the

form:

$$H_{\text{NRQM}} = \sum_{i=1}^3 (m_i + T_i) - T_G + \sum_{i<j} V_{ij}(r_{ij}) + C_0, \quad (16)$$

where m_i and T_i denote the constituent quark mass and kinetic energy of the i -th quark, respectively. T_G is the center-of-mass kinetic energy and C_0 is the zero point energy. The term V_{ij} represents the effective potential between the i -th and j -th quarks with a distance $r_{ij} \equiv |\mathbf{r}_i - \mathbf{r}_j|$. The potential incorporates both the confinement interaction and the OGE contribution, which can be decomposed into spin-independent and spin-dependent components:

$$V_{ij}(r_{ij}) = V_{ij}^{\text{si}}(r_{ij}) + V_{ij}^{\text{sd}}(r_{ij}). \quad (17)$$

The spin-independent term V_{ij}^{si} is composed of a linear and Coulomb potential:

$$V_{ij}^{\text{si}}(r_{ij}) = \frac{b}{2} r_{ij} - \frac{2}{3} \frac{\alpha_s}{r_{ij}}, \quad (18)$$

where the parameter b represents the strength of the confinement and α_s the strong coupling constant. The spin-dependent term comprises spin-spin, spin-orbit and tensor potentials:

$$V_{ij}^{\text{sd}} = V_{ij}^{\text{SS}} + V_{ij}^{\text{LS}} + V_{ij}^{\text{T}}. \quad (19)$$

For the spin-spin and tensor terms, we adopt the widely used forms:

$$V_{ij}^{\text{SS}} = -\frac{2\alpha_s}{3} \left\{ -\frac{\pi}{2} \frac{\sigma_{ij}^3 e^{-\sigma_{ij}^2 r_{ij}^2}}{\pi^{3/2}} \cdot \frac{16}{3 m_i m_j} (\mathbf{S}_i \cdot \mathbf{S}_j) \right\}, \quad (20)$$

$$V_{ij}^{\text{T}} = \frac{2\alpha_s}{3} \frac{1}{m_i m_j r_{ij}^3} \left\{ 3 \frac{(\mathbf{S}_i \cdot \mathbf{r}_{ij})(\mathbf{S}_j \cdot \mathbf{r}_{ij})}{r_{ij}^2} - \mathbf{S}_i \cdot \mathbf{S}_j \right\}, \quad (21)$$

where \mathbf{S}_i is the spin operator of the i -th quark, and σ_{ij} is the smearing parameter introduced to regulate the short-range contact interaction. For the spin-orbit interaction, we employ the simplified phenomenological form used in Ref. [45] (originally proposed in Refs. [46, 47]), which is

$$V_{ij}^{\text{LS}} = \frac{\alpha_{\text{SO}}}{\rho^2 + \lambda^2} \cdot \frac{\mathbf{L} \cdot \mathbf{S}}{3(m_1 + m_2 + m_3)^2}, \quad (22)$$

where \mathbf{L} and \mathbf{S} correspond to the total orbital and total spin angular momentum of the baryon respectively, and α_{SO} is the spin-orbit coupling strength.

2. Numerical method

The bare masses and spatial wave functions could be obtained by numerically solving the Schrödinger equation with the Hamiltonian above. For such a three-body system, the

total spatial wavefunction $\psi_{NLM_L}(\boldsymbol{\rho}, \boldsymbol{\lambda})$ can be expanded as a combination of $\psi_{n_\rho l_\rho m_\rho}(\boldsymbol{\rho})$ and $\psi_{n_\lambda l_\lambda m_\lambda}(\boldsymbol{\lambda})$,

$$\Psi_{NLM_L}(\boldsymbol{\rho}, \boldsymbol{\lambda}) = \sum_{\substack{N=2(n_\rho+n_\lambda) \\ +l_\rho+l_\lambda \\ L=l_\rho+l_\lambda}} C_{n_\rho l_\rho m_\rho}^{n_\lambda l_\lambda m_\lambda} [\psi_{n_\rho l_\rho m_\rho}(\boldsymbol{\rho}) \psi_{n_\lambda l_\lambda m_\lambda}(\boldsymbol{\lambda})]_{NLM_L}, \quad (23)$$

where $\boldsymbol{\rho}$ describes the relative motion between two quarks, and $\boldsymbol{\lambda}$ the motion of the third quark relative to the quark-pair center of mass. The n_ρ and n_λ are the principal quantum numbers of the ρ - and λ -mode oscillators, respectively, while the N, L and M are the total principal quantum number, the total orbital quantum number and its z component, respectively. The ρ - and λ -mode spatial wave functions share the common decomposition:

$$\psi_{n_\ell l_\ell m_\ell}(\boldsymbol{\xi}) = R_{n_\ell l_\ell}(\xi) Y_{l_\ell m_\ell}(\hat{\boldsymbol{\xi}}), \quad (24)$$

with the radial part $R_{n_\ell l_\ell}(\xi)$ and the angular dependence encoded in the spherical harmonic $Y_{l_\ell m_\ell}(\hat{\boldsymbol{\xi}})$. In this work, we employ the multi-Gaussian expansion method (GEM) to calculate the hadron mass spectrum and the radial wave functions. Unlike the conventional Gaussian expansion method proposed by Hiyama et al. [48], our trial radial wave functions $R_{n_\ell l_\ell}(\xi)$ are expanded with a series of harmonic oscillator functions:

$$R_{n_\ell l_\ell}(\xi) = \sum_{l=1}^n C_{\xi l} \phi_{n_\ell l_\ell}(d_{\xi l}, \xi), \quad (25)$$

where

$$\begin{aligned} \phi_{n_\ell l_\ell}(d_{\xi l}, \xi) &= \left(\frac{1}{d_{\xi l}} \right)^{\frac{3}{2}} \left[\frac{2^{l_\ell+2-n_\ell} (2l_\ell+2n_\ell+1)!!}{\sqrt{\pi} n_\ell! [(2l_\ell+1)!!]^2} \right]^{\frac{1}{2}} \left(\frac{\xi}{d_{\xi l}} \right) \\ &\times e^{-\frac{1}{2} \left(\frac{\xi}{d_{\xi l}} \right)^2} F\left(-n_\ell, l_\ell+3/2, \left(\frac{\xi}{d_{\xi l}} \right)^2\right), \end{aligned} \quad (26)$$

where $F(-n_\ell, l_\ell+3/2, (\xi/d_{\xi l})^2)$ is the confluent hypergeometric function. The variational parameter $d_{\xi l}$ is related to the harmonic oscillator frequency $\omega_{\xi l}$ via

$$\frac{1}{d_{\xi l}^2} = M_\xi \omega_{\xi l}. \quad (27)$$

The reduced masses are defined by

$$M_\rho \equiv \frac{2m_1 m_2}{m_1 + m_2}, \quad M_\lambda \equiv \frac{3(m_1 + m_2)m_3}{2(m_1 + m_2 + m_3)}. \quad (28)$$

On the other hand, the harmonic oscillator frequency $\omega_{\xi l}$ can be related to the oscillator stiffness constant K_l through

$$\omega_{\xi l} = \sqrt{\frac{3K_l}{M_\xi}}. \quad (29)$$

Thus, for an udd system, we can easily obtain the following equation:

$$d_{\rho l} = d_{\lambda l} = d_l = (3m_u K_l)^{-1/4}, \quad (30)$$

where m_u is the constituent mass of the up quark.

Concerning the determination of the variational parameters, we adopt the procedure of Hiyama et al. [48], in which the parameters are selected according to a geometric progression,

$$d_\ell = d_1 a^{\ell-1} \quad (l = 1, 2, \dots, n). \quad (31)$$

It is found that when we take $d_1=0.1$ fm, $d_n=2$ fm and $n=15$, stable solutions for the N baryons could be obtained. Finally, the Schrödinger equation can be solved by dealing with the generalized eigenvalue problem,

$$\sum_{\ell=1}^n \sum_{\ell'=1}^n (H_{\ell\ell'} - E_\ell N_{\ell\ell'}) C_{\ell'}^\ell = 0, \quad (32)$$

where the Hamiltonian elements between different Gaussian bases and the overlapping matrix element of the Gaussian bases are respectively expressed as

$$H_{\ell\ell'} \equiv \langle \Psi(d_{\ell'}) | H | \Psi(d_\ell) \rangle, \quad N_{\ell\ell'} \equiv \langle \Psi(d_{\ell'}) | \Psi(d_\ell) \rangle. \quad (33)$$

C. The Quark Pair Creation Model

We adopt the Quark Pair Creation (QPC) model to describe the coupling vertices $f_i(E)$ between the bare baryon state and the meson–baryon continuum. These vertices are expressed as $f_{SL}(E)$ where the subscripts S and L denote the total spin and relative angular momentum of the scattering channel respectively. The QPC model has a long history of success in

describing the OZI-allowed strong decay process of mesons and baryons [49–51], providing analytical forms for the vertex functions. Motivated by the successful application of the QPC model to the charmonium system in our previous work [52], we extend this framework to the nucleon sector, allowing for a straightforward and consistent extraction of the $N^* \rightarrow$ meson–baryon coupling vertices within the extended Lee-Friedrichs scheme.

In the QPC model, the transition operator for the process $A \rightarrow BC$ in the non-relativistic framework is given by

$$T = -3\gamma \sum_m \langle 1m; 1-m | 00 \rangle \int d^3\mathbf{p}_4 d^3\mathbf{p}_5 \delta^3(\mathbf{p}_4 + \mathbf{p}_5) \times \mathcal{Y}_1^m \left(\frac{\mathbf{p}_4 - \mathbf{p}_5}{2} \right) \chi_{45}^{1,-m} \phi_{45}^0 \omega_{45}^0 a_4^\dagger(\mathbf{p}_4) b_5^\dagger(\mathbf{p}_5), \quad (34)$$

where γ is a dimensionless vacuum production strength parameter and $a_4^\dagger(\mathbf{p}_4) b_5^\dagger(\mathbf{p}_5)$ create a quark-antiquark pair with momenta \mathbf{p}_4 and \mathbf{p}_5 . $\mathcal{Y}_1^m(\mathbf{p}) = |\mathbf{p}| Y_1^m(\theta_p, \phi_p)$ is the solid harmonic polynomial reflecting the momentum-space distribution. ω_{45}^0 , ϕ_{45}^0 and $\chi_{45}^{1,-m}$ denote the color, flavor singlets and spin triplet factor of the quark pair, respectively. These components ensure the created quark pair carries the vacuum quantum number $J^{PC} = 0^{++}$.

By standard derivation, the partial-wave transition amplitude of $A \rightarrow BC$ can be represented as

$$M_{A \rightarrow BC}^{SL}(\mathbf{P}) = \gamma \sqrt{\frac{4\pi(2L+1)}{2J_A+1}} \sum_{M_{J_B} M_{J_C}} \langle L0; S(M_{J_B} + M_{J_C}) | J_A(M_{J_B} + M_{J_C}) \rangle \langle J_B M_{J_B} J_C M_{J_C} | S(M_{J_B} + M_{J_C}) \rangle \times \Pi_{A,B,C} \langle \chi_{S_B M_{S_B}}^{12,4} \chi_{S_C M_{S_C}}^{3,5} | \chi_{S_A M_{S_A}}^{1,2,3} \chi_{1-m}^{4,5} \rangle \langle \phi_B^{12,4} \phi_C^{3,5} | \phi_A^{1,2,3} \phi_0^{4,5} \rangle I_{M_{L_B}, M_{L_C}}^{M_{L_A}, m}(\mathbf{P}) \quad (35)$$

with \mathbf{P} representing the three-momentum of particle B in the c.m. frame of particle A . The $I_{M_{L_B}, M_{L_C}}^{M_{L_A}, m}(\mathbf{P})$ are the spatial overlaps of the initial and final states, which can be written as

$$I_{M_{L_B}, M_{L_C}}^{M_{L_A}, m}(\mathbf{P}) = \int d^3\mathbf{p}_1 d^3\mathbf{p}_2 d^3\mathbf{p}_3 d^3\mathbf{p}_4 d^3\mathbf{p}_5 \delta^{(3)}(\mathbf{p}_1 + \mathbf{p}_2 + \mathbf{p}_3 - \mathbf{p}_A) \delta^{(3)}(\mathbf{p}_1 + \mathbf{p}_4 + \mathbf{p}_3 - \mathbf{p}_B) \delta^{(3)}(\mathbf{p}_2 + \mathbf{p}_5 - \mathbf{p}_C) \delta^{(3)}(\mathbf{p}_4 + \mathbf{p}_5) \times \psi_{n_B M_{L_B}}^*(\mathbf{p}_1, \mathbf{p}_4, \mathbf{p}_3) \psi_{n_C M_{L_C}}^*(\mathbf{p}_2, \mathbf{p}_5) \psi_{n_A M_{L_A}}(\mathbf{p}_1, \mathbf{p}_2, \mathbf{p}_3) \mathcal{Y}_{1m} \left(\frac{\mathbf{p}_4 - \mathbf{p}_5}{2} \right),$$

and $\Pi_{A,B,C}$ accounts for the sum over intermediate magnetic indices with the relevant Clebsch–Gordan coefficients as

$$\Pi_{A,B,C} \rightarrow \sum_{\substack{M_{L_A}, M_{S_A}, M_{L_B}, M_{S_B} \\ M_{L_C}, M_{S_C}, m}} \langle L_A M_{L_A} S_A M_{S_A} | J_A(M_{J_B} + M_{J_C}) \rangle \times \langle L_B M_{L_B} S_B M_{S_B} | J_B M_{J_B} \rangle \times \langle L_C M_{L_C} S_C M_{S_C} | J_C M_{J_C} \rangle \langle 1, m; 1, -m | 0, 0 \rangle. \quad (36)$$

It is worth mentioning that here the simple harmonic oscillator (SHO) wave functions are employed in spatial integration,

$$\psi_{n_\rho, n_\lambda}(l_\rho, m_\rho, l_\lambda, m_\lambda) = 3^{3/4} (-i)^{2n_\rho + l_\rho} \sqrt{\frac{2n_\rho!}{\Gamma(n_\rho + l_\rho + 3/2)}} \left(\frac{1}{\alpha_\rho} \right)^{3/2 + l_\rho} L_{n_\rho}^{l_\rho + 1/2} \left(\frac{\mathbf{p}_\rho^2}{\alpha_\rho^2} \right) e^{-\mathbf{p}_\rho^2 / (2\alpha_\rho^2)} \mathcal{Y}_{l_\rho}^{m_\rho}(\mathbf{p}_\rho) \times (-i)^{2n_\lambda + l_\lambda} \sqrt{\frac{2n_\lambda!}{\Gamma(n_\lambda + l_\lambda + 3/2)}} \left(\frac{1}{\alpha_\lambda} \right)^{3/2 + l_\lambda} L_{n_\lambda}^{l_\lambda + 1/2} \left(\frac{\mathbf{p}_\lambda^2}{\alpha_\lambda^2} \right) e^{-\mathbf{p}_\lambda^2 / (2\alpha_\lambda^2)} \mathcal{Y}_{l_\lambda}^{m_\lambda}(\mathbf{p}_\lambda) \quad (37)$$

The harmonic oscillator parameters $\alpha_{\rho/\lambda}$ are determined by matching the effective radius of the full wave function expanded in 15 sets of Gaussians with that of SHO wave function, such that

$$\sum_{i,j=1}^{15} N_{\text{nor}} \cdot c_j^* c_i \langle \phi_j | \rho^2 | \phi_i \rangle = \langle \Psi_{\text{SHO}} | \rho^2 | \Psi_{\text{SHO}} \rangle. \quad (38)$$

Consequently, the SHO wave function accurately approximates the spatial extent of the full wave function, and can be utilized directly in calculating the coupling vertices. This approach significantly enhances the computational efficiency of the integral evaluation with the η function during the pole-searching procedure.

The momentum \mathbf{P} is the the three momentum of the final-state particle in the initial-state rest frame, given by $|\mathbf{P}(E)| = \lambda(E^2, M_B^2, M_C^2)^{1/2}/(2E)$ where $\lambda(x, y, z) = x^2 + y^2 + z^2 - 2xy - 2yz - 2xz$ is the Källén function. Then, the coupling vertex function $f_{SL}(E)$ in Eq. (8), which describes the interaction between $|1\rangle$ and $|E_i\rangle$ in the extended Lee-Friedrichs scheme, can be obtained as

$$f_{SL}(E) = \sqrt{\mu P(E)} M_{SL}(P(E)), \quad (39)$$

where $\sqrt{\mu P(E)}$ is a phase-space factor and $\mu = (E_B E_C)/(E_B + E_C)$ is the reduced mass of the two-body system.

To regulate the high energy behavior of the QPC coupling of the dispersion relation integral, once-subtracted dispersion relation is used in calculating the η function as

$$\eta(x) = x - m_0 - (s_0 - x) \sum_{i,S,L} \int_{\omega_{th,i}}^{\infty} \frac{|f_{SL}(E)|^2}{(x - E)(s_0 - E)} dE, \quad (40)$$

where s_0 is taken at the threshold $\omega_{th,N\pi}$. In this formulation, the subtraction constant is implicitly absorbed into the bare mass of the bare N^* state.

III. NUMERICAL ANALYSIS

The approach differs from the conventional strategy for resonance studies. Usually, the potential model parameters are typically determined by fitting the predicted eigenvalues to the physical mass spectrum, with decay widths subsequently calculated through a decay model in a separate procedure. In this study, we used the potential model to generate the bare mass spectrum and the wave functions, which serve as input of bare masses and the coupling vertices in the extended LF scheme. By fitting the resulting pole masses and widths to experimental data of all the $1S$ and $1P N^*$ states, we determined the potential model parameters and the vacuum production strength γ . Using these determined values, we subsequently calculated the pole position of the $2S$ state, which can be considered a theoretical prediction of this framework.

The coupled channels chosen in the analysis include πN , $\Delta\pi$ and ηN , which are the leading decay modes of $1P$ - and $2S$ -wave nucleons as listed in the PDG table. While an infinite

tower of channels with matching quantum numbers could, in principle, couple to a given state, we assume that contributions from higher-mass virtual loops are effectively absorbed into the parameters of the quark potential model or suppressed by the once-subtracted dispersion relation. Although including sub-dominant channels is feasible in principle, the resulting proliferation of branch cuts and Riemann sheets would render the numerical identification of poles increasingly inefficient.

In the numerical calculation, the masses and wave functions of nucleons are obtained by solving the Hamiltonian eigenfunction in the potential model with the GEM. To facilitate further calculation of coupling vertices in the LF scheme, we determine an effective oscillator parameter $\alpha_{\rho/\lambda}$ by matching the root-mean-square radius with that of SHO basis. Consequently, the coupling vertices between the nucleon and the continuum states in the LF scheme can be expressed in an analytical form, which significantly improves the efficiency in searching poles on the complex plane.

The potential parameters and the vacuum production strength γ are determined by matching the predicted complex poles to experimental values. Since these parameters are fixed at the pole level, they implicitly account for coupled-channel dynamics. This optimized parameter set is then applied to the $2S$ state to explore the properties of higher nucleon excitations within the same formalism.

Parameter	Value	Parameter	Value
b	0.10 ± 0.03	α_{SO}	0.61 ± 0.20
α	1.06 ± 0.22	C_0	-0.35 ± 0.30
σ	0.66 ± 0.17	γ	6.52 ± 0.49

TABLE I: Parameters in potential model and QPC model.

Our theoretical framework involves six free parameters. Five of them are associated with the potential model—namely, the confinement parameter b , the strong coupling constant α_s , the smearing parameter σ , the spin-orbit coefficient α_{SO} , and the zero-point constant C_0 . The sixth is the dimensionless coupling strength γ , which characterizes the QPC vertex. The constituent quark mass of u/d is empirically fixed at 0.35 GeV. These parameters are determined by fitting the mass of the ground state and the pole positions of the $1P$ -wave nucleons given by PDG [21]. The resultant optimal parameter set is summarized in Table I.

Using the parameter set, we calculate the mass and pole positions of the ground state of the $1P$ - and $2S$ -wave nucleons, as listed in Table III, where n represents the principal quantum number with $n = 1$ corresponding to the ground state. To further investigate the dynamical origin of these poles, we trace their trajectories in relevant physical and un-physical sheets in Fig. 2, as the vacuum coupling parameter changes.

The LF model provides an exactly solvable framework that explicitly incorporates the properties of Gamow states, and it allows for a explicit representation of the resonance wave function in RHS, as shown in Eq. (15). Beyond the pole positions and trajectories, the internal nature of a hadronic state is often characterized by its elementariness (Z) and composite-

ness (X). However, some theoretical subtleties regarding their interpretation must be noted.

For a stable bound state case, the elementariness Z and compositeness coefficients X_i represents the probability of finding the bare discrete state and the i -th continuum state, respectively, within the physical state $|z_B\rangle$ (see Eq. (13)). The elementariness and compositeness are defined as

$$Z = N_B^2, \quad X_i = N_B^2 \int_{\omega_{\text{th},i}}^{\infty} \frac{|f_i(E)|^2 dE}{(z_B - E)^2}. \quad (41)$$

The bound-state energy z_B is real and situated below the lowest threshold, and Z and X_i are both real, satisfying the normalization condition $Z + \sum_i X_i = 1$. As such, they admit a standard probability explanation [53–55].

However, for the resonance state, one can define analogous quantities Z' and X'_i as

$$Z' = N_R^2, \quad X'_i = N_R^2 \int_{\omega_{\text{th},i}}^{\infty} \frac{|f_i(E)|^2 dE}{[z_R - E]_+^2}. \quad (42)$$

While this definition is formally plausible, the required deformation of integration contour into the unphysical RS renders Z' and X'_i complex-valued. As a result, they no longer possess a direct probability explanation [35]. To adopt a qualitative measure of resonance composition, different methods for evaluating the quantities of resonances were discussed in detail in the Ref. [56]. Here, we adopt the following prescription based on the absolute value of these coefficients

$$\tilde{Z} \equiv \frac{|Z'|}{\sum_i |X'_i| + |Z'|}, \quad \tilde{X}_i \equiv \frac{|X'_i|}{\sum_i |X'_i| + |Z'|}. \quad (43)$$

Alternative approaches to define elementariness and compositeness for resonance could be found in literature, such as Ref. [57–60]. These measures of elementariness and compositeness provide a qualitative means to differentiate bare-state dominance from continuum-driven dynamics. Such a classification sheds light on the formation mechanisms and the internal nature of the poles listed in Table III. We will address the properties of these states in the following.

A. $N(1440) J^P = 1/2^+$

Within this framework, using the parameters determined from the $1P$ -wave section, the bare mass of $2S$ state is predicted to be 1.8 GeV. This value is consistent with typical constituent quark model expectations from the first radial excitation of the nucleon. However, the physical $N(1440)$ resonance appears at a much lower mass. As illustrated by the pole trajectory in Fig. 2, the inclusion of coupled-channel dynamics leads to significant mass renormalization, where the arrow indicates that the pole moves downward as the coupling strength increases. As the coupling strength γ to the πN , $\pi\Delta$ and ηN channels is gradually increased to the fitted value of 6.52, the $2S$ pole moves drastically downward from its bare position, and eventually resides at $(\text{Re } M_R, -\text{Im } M_R) = (1.487, 0.070)$ GeV, which is close the $N(1440)$ listed by PDG. This

substantial shift of approximately 320 MeV demonstrated that the roper resonance is highly non-perturbative object, where the interaction with the meson-baryon continuum plays a decisive role in forming the physical mass and width.

A long-standing puzzle in baryon spectroscopy is the “level-inversion” problem, where the $N(1440)$ is experimentally observed to be lighter than the $N(1520)$ and $N(1535)$ states, a feature that contradicts the conventional quark models. Our results show that the meson-baryon cloud induced by the coupled channel effect might be a key mechanism for resolving the level-inversion difficulty, as the $2S$ state exhibits a much higher sensitivity to the continuum dressing than the $1P$ states.

The internal structure of $N(1440)$ might be further studied by the approximated elementariness \tilde{Z} and compositeness \tilde{X}_i listed in Table III. Due to the complex nature of these coefficients for resonances, we employ the normalized absolute-value prescription for a qualitative assessment. We find that the bare-state fraction \tilde{Z} is less than 40%, close to the result of 36.9% reported in Ref. [32]. This low value of \tilde{Z} also indicate that the Roper resonance is not a pure three-quark state but is instead predominantly composite. Physically, it can be viewed as a bare three-quark core surrounded by a dense meson-baryon cloud, with the πN and $\pi\Delta$ components provide dominant compositeness. This picture is consistent with recent analyses from Refs. [2, 61]. However, the dynamical model in Ref. [2] suggests that, due to strong coupled-channel effects, the same bare state also induces a relatively broad resonance around 1.8 GeV, potentially associated with the $N(1710)$. In our theoretical framework, we have not found the signal of such a higher-mass resonance. This difference might be attributed to the specific form of the vertex functions or the channel space. It suggests that the high-energy behavior of the transition potentials or the interference between different partial waves might contribute to additional shadow pole structure.

B. $N(1535)$ and $N(1650) J^P = 1/2^-$

The internal nature of the $N(1535)$ resonance has long been a subject of theoretical debate. Within the chiral unitary approach with a natural renormalization scheme, Ref. [62] argued that the $N(1535)$ resonance contains a significant genuine quark component, distinguishing it from states like $\Lambda(1405)$ which are considered to be predominantly dynamically generated. This result is supported by the Jülich-Bonn dynamical coupled-channel approach [28]. However, the degree of its “elementariness” remains a point of contention.

Alternatively, other studies based on chiral effective other studies based on SU(3) chiral effective Lagrangian theories suggest that $N(1535)$ can be generated primarily through meson-baryon dynamics, without the need of introducing an explicit s-channel bare state, but rather as a consequence of the non-perturbative resummation of coupled-channel interactions. In these approaches, the strong couplings to the KA and $K\Sigma$ channels are found to play a particularly important role in the formation of the resonance, which indicates that

Notation	Bare mass	Pole	State	PDG (BW)	PDG (Poles)	Ref. [32]	Ref. [2]
$1^2P_{1/2^-}$	1.656	$1.631 - 0.065i$	$N(1535)$	$1.530 - 0.075i$	$1.510 - 0.055i$	$1.504 - 0.037i$	$1.540 - 0.191i$
$1^2P_{3/2^-}$	1.691	$1.528 - 0.063i$	$N(1520)$	$1.515 - 0.055i$	$1.510 - 0.055i$	$1.482 - 0.063i$	$1.521 - 0.058i$
$1^4P_{1/2^-}$	1.621	$1.610 - 0.043i$	$N(1650)$	$1.650 - 0.063i$	$1.665 - 0.067i$	$1.678 - 0.064i$	$1.642 - 0.041i$
$1^4P_{3/2^-}$	1.839	$1.842 - 0.129i$	$N(1700)$	$1.720 - 0.100i$	$1.700 - 0.100i$	–	–
$1^4P_{5/2^-}$	1.802	$1.677 - 0.013i$	$N(1675)$	$1.675 - 0.074i$	$1.655 - 0.067i$	$1.652 - 0.060i$	$1.654 - 0.077i$
$2^2S_{1/2^+}$	1.799	$1.487 - 0.070i$	$N(1440)$	$1.440 - 0.175i$	$1.370 - 0.085i$	$1.353 - 0.102i$	$1.364 - 0.105i$

TABLE II: Pole positions of selected N^* states. The unit is GeV.

State	Z	\tilde{Z}	$X_{\pi N}$	$\tilde{X}_{\pi N}$	$X_{\pi\Delta}$	$\tilde{X}_{\pi\Delta}$	$X_{\eta N}$	$\tilde{X}_{\eta N}$
$N(1535)$	$0.65 + 0.15i$	47.5%	$0.08 - 0.18i$	13.7%	$0.37 + 0.14i$	27.9%	$-0.11 - 0.11i$	10.8%
$N(1520)$	$0.74 - 0.30i$	56.3%	$0.28 + 0.08i$	20.7%	$-0.08 + 0.25i$	18.6%	$0.05 - 0.03i$	4.4%
$N(1650)$	$1.08 + 0.12i$	70.9%	$0.01 - 0.07i$	4.5%	$0.13 + 0.03i$	9.0%	$-0.22 - 0.09i$	15.6%
$N(1700)$	$0.52 + 0.19i$	50.8%	$-0.00 + 0.01i$	0.7%	$0.48 - 0.21i$	47.6%	$0.00 + 0.01i$	0.9%
$N(1675)$	$0.61 - 0.13i$	60.0%	$0.02 + 0.03i$	3.3%	$0.34 + 0.09i$	33.4%	$0.03 + 0.01i$	3.3%
$N(1440)$	$0.44 - 0.25i$	39.6%	$0.11 + 0.30i$	25.0%	$0.41 - 0.06i$	32.6%	$0.04 + 0.00i$	2.8%

TABLE III: The compositeness and elementariness of selected N^* states.

the possibility of the $N(1535)$ being a dynamically generated state cannot be ruled out [63–66].

In our LF framework, by introducing a bare state $1^2P_{1/2^-}$, we find a resonance in the complex plane at $(\text{Re } M_R, -\text{Im } M_R) = (1.631, 0.063)$ GeV. This result, while slightly higher than the PDG average, is remarkably consistent with the result of Hamiltonian effective field theory in Ref. [67], which gives $(\text{Re } M_R, -\text{Im } M_R) = (1.602, 0.089)$ GeV. The discrepancy with PDG values may arise from the simplified treatment of high-energy tails of the vertex functions. Nevertheless, our compositeness analysis in Table III provide a clear structural distinction: the $N(1535)$ exhibits a significantly larger compositeness compared to the $N(1650)$, which remains relatively compact. This conclusion aligns with the spectral density analysis in Ref. [32].

We also observe that $N(1535)$ and $N(1650)$ are nearly degenerate in our calculation. According to the PDG [21], these two states not only share the same quantum numbers $J^P = 1/2^-$ but also exhibit similar dominant decay channels, particularly into the πN and ηN channels. It is therefore physically motivated to interpret these two states as the physical manifestations of the mixing between the $1^2P_{1/2^-}$ and $1^4P_{1/2^-}$ bare configurations. The mixing angle can be extracted from the photoproduction data (often reported as $25^\circ \sim 30^\circ$), such as $\gamma p \rightarrow \eta p$ [68] and $\gamma p \rightarrow \pi^0 p$ [34, 69].

In the limit of exact SU(6) symmetry, these two states would be degenerate. However, the inclusion of spin-dependent interactions breaks the symmetry, inducing mixing between the two states. In Ref. [19], a comparable mixing angle of approximately $\theta = 26^\circ$ can also be obtained by in-

roducing OGE and OBE potentials and considering the mixing between these two states via the tensor interaction. The mixing mechanism can also provide a phenomenological explanation for the distinct branching fractions of $N(1535)$ and $N(1650)$ into πN and ηN channels [19].

In the present framework, by phenomenologically adopting this mixing angle $\theta = 26^\circ$, the positions of these two poles will shift to $(\text{Re } M_R, -\text{Im } M_R) = (1.649, 0.074)$ GeV and $(\text{Re } M_R, -\text{Im } M_R) = (1.603, 0.041)$ GeV, respectively. It is evident that they appear to split further, suggesting that the experimentally observed states are more preferably understood as linear combinations of multiple underlying states. This splitting also indicates that the dynamical coupling to meson-baryon continua and the internal spin-flavor mixing are inextricably linked, both contributing to the observed mass spectrum and decay patterns of the S_{11} nucleon resonances.

C. $N(1520)$ and $N(1700)$ $J^P = 3/2^-$

In the traditional quark model, the $N(1520)$ and $N(1700)$ are classified as the $1P$ -wave excited nucleons with $J^P = 3/2^-$, corresponding to the $1^2P_{3/2^-}$ and $1^4P_{3/2^-}$ configurations, respectively. Based on the qualitative decomposition as introduced in Eq. (43), our calculations yield bare-state fractions of approximately 50% for both states. These results suggest that the $N(1520)$ and $N(1700)$ state exhibits a significant composite nature, where meson-baryon components plays a non-negligible role in their formation. This findings for $N(1520)$ is consistent with the spectral density analysis presented in

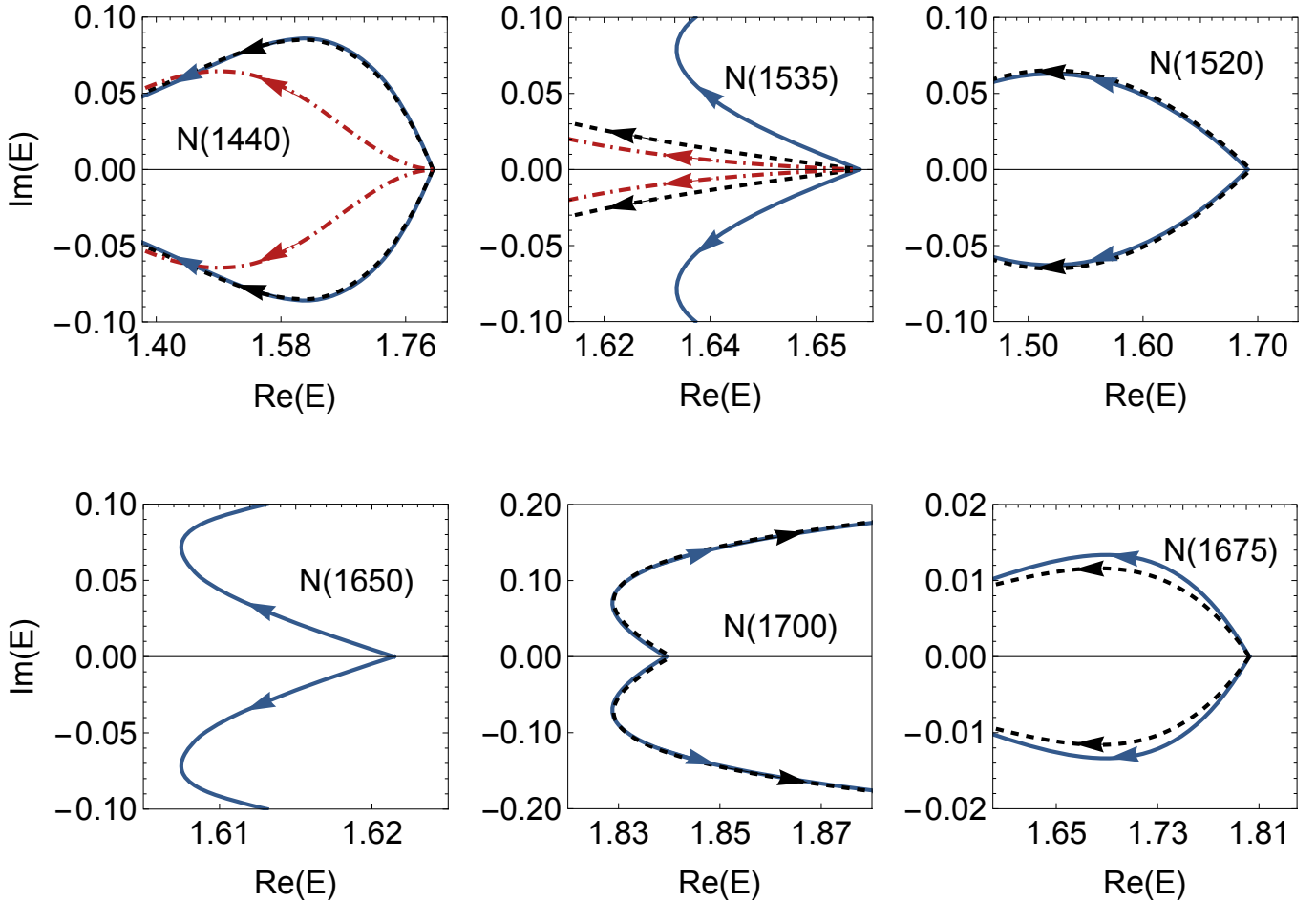


FIG. 2: Pole trajectories with the arrow indicating the moving direction when the coupling strength increases. The blue solid, black dashed, and red dash-dotted curves represent the pole trajectories on the fourth, third, and second Riemann sheets, respectively. The unit is GeV.)

Ref. [32].

A particularly compelling piece of evidence for our model's validity is found in the channel-specific compositeness values \tilde{X}_i . We find that $N(1520)$ is dominated by a large πN component, whereas $N(1700)$ is characterized by a predominant $\pi\Delta$ compositeness. This aligns remarkably well with the PDG branch fractions [21], which indicate that $N(1520)$ decays primarily to the πN channel (55 ~ 65%) while $N(1700)$ is known to have a significant decay width into the $\pi\Delta$ channel. This agreement reinforces the physical relevance of the estimated composition, which suggests that each bare state preferentially dresses itself with specific meson-baryon clouds that reflect its underlying spin-flavor structure.

Differ from the other states discussed here, $N(1700)$ is the only 3-star broad resonance in the PDG, which has larger uncertainties in pole positions. In this LF scheme, $N(1700)$ appears as a robust and stable resonance together with the $N(1520)$, despite its weak πN (d-wave) signals and large experimental uncertainties. Due to the strong coupling of the $1^4P_{3/2^-}$ bare state to the continua, its pole moves from the real axis to the complex energy plane and then shift rapidly upwards as the coupling constant γ increases, eventually ap-

pearing as a broad resonance pole centered around 1800 MeV with a width of approximately 260 MeV.

Intriguingly, as the coupling increases, besides the emergence of $N(1700)$, a dynamically generated state arises from a distant region, eventually settles on the complex $(\text{Re } M_R, -\text{Im } M_R) = (1.468, 0.236)$ GeV in the third Riemann sheet. Since this pole is located on the complex energy plane when the coupling constant γ tends to zero, it implies the molecule origin of this state, that means this pole is predominantly generated by the meson-baryon dynamics rather than a bare quark core. However, its extremely large width ($\Gamma > 470$ MeV) may explain why this dynamical generated state may bring challenges to its experimental observation due to the feature of $\Gamma > 300$ MeV. This analogous mechanism, two pole structure, frequently occurs in meson systems, such as $f_0(500)$ and $K_0^*(700)$ [70]. It is noteworthy that a similar dynamical generated state found $(\text{Re } M_R, -\text{Im } M_R) = (1.467, 0.083)$ GeV, corresponding to $N(1520)$ in Ref. [71]. This state has a comparable mass with ours but a significantly narrower width.

Similarly, for these two states sharing the same quantum numbers, incorporation a more refined three-body spin-orbit potential, as detailed in Ref. [19], allows for a direct compu-

tation of the mixing angle, yielding $\theta = 20^\circ$. By adopting this mixing angle as input, due to the strong coupling of the ${}^4P_{3/2}$ -state, the pole positions after mixing shift significantly, locating at $(\text{Re } M_R, -\text{Im } M_R) = (1.466, 0.098)$ GeV and $(\text{Re } M_R, -\text{Im } M_R) = (1.714, 0.073)$ GeV, corresponding to $N(1520)$ and $N(1700)$, respectively. The new position of $N(1520)$ is close to the result in Ref. [71], while the pole position of $N(1700)$ shows improved consistency with the PDG averaged values.

D. $N(1675) J^P = 5/2^-$

For the $N(1675)$ resonance state, the calculated pole width is somewhat narrower than experimental value reported by the PDG. This discrepancy likely originates from several factors. First, the transition couplings derived from the QPC model may carry inherent uncertainties, which directly affect the imaginary of the self energy. Second, our current calculation only incorporates the three most dominant decay channels. Other channels, such as ρN , ωN and $K\Sigma$, though smaller in branching fractions, may vary the pole position.

According to Ref. [32], more channels were considered, and the composition of each configuration was analyzed. Their results indicate that the ρN channel contributes approximately 10% for this state. When multiple decay channels are included, as three channels in the present case, the pole trajectories generally exhibit more complicated behavior. In particular, interference effects among different channels can reduce the total decay probability, which may lead to a narrower pole width compared with the single-channel case. The complex amplitudes from various channels can partially cancel each other in the imaginary part of the pole position, reflecting the underlying multichannel dynamics rather than a simple sum of individual widths. Instead of pursuing an exact agreement with the experimental width, we focus more on the pole trajectories.

IV. SUMMARY

In this work, we have investigated the pole structure and Gamow-state compositions of low-lying nucleon resonances within an extended LF scheme. By integrating the bare states of selected resonance and their coupling to meson-baryon continuum states described by the QPC model, we constructed a multi-channel framework including the πN , $\pi\Delta$ and ηN continua. These three dominant channels are selected to capture

the essential dynamics of the system. The model parameters are calibrated by matching the pole masses and widths with those values of the $1P$ -wave resonances documented by PDG.

Our framework successfully reproduces six resonances are successfully reproduced, $N(1535)1/2^-$, $N(1520)3/2^-$, $N(1650)1/2^-$, $N(1700)3/2^-$, $N(1675)5/2^-$ and $N(1440)1/2^+$. By tracing the pole trajectories and analyzing their elementariness and compositeness, we demonstrate that the strong coupling between the $2S$ state and these channels contributes a significant mass shift, and then generating a broad resonance around 1.4 GeV. Specifically, the elementariness of $N(1440)$ is found to be less than 40%, which suggests that it is not a pure valence quark state but rather a three-quark core heavily dressed by baryon-meson clouds. This implies that incorporating unquenched effects into the traditional quark model is promising in understanding the internal structures of excited nucleons and resolving the long-standing mass-inversion puzzle. In addition, a dynamically generated $J^P = 3/2^-$ state with a pole position at $(\text{Re } M_R, -\text{Im } M_R) = (1.468, 0.236)$ GeV. This state is likely to appear accompanied with $N(1700)$, though its large width likely poses a challenge for clear experimental identification.

Despite these successes, we acknowledge that certain uncertainties remain between our pole positions and the PDG values. These uncertainties might stem from three primary aspects: Firstly, the QPC model employed for the coupling vertex functions represents a leading-order approximation; Moreover, the values for the masses and widths of these resonances listed by PDG are averages with sizable uncertainties, which may propagate into our parameter determination; Lastly, some higher-order coupled channels were omitted to maintain computational tractability.

This study represents our first application of the extended LF framework to the complex dynamics of the baryon system. The results demonstrate the feasibility and robustness of this approach in describing the unquenched baryon spectrum. Further work will focus on refining the vertex functions and extending this systematic investigation to other baryon sections.

Acknowledgement

Helpful discussion with Zhi-Guang Xiao are appreciated. This work is supported by China National Natural Science Foundation under contract Nos. 12375132, 11975075 and 12175065.

-
- [1] L. David Roper. Evidence for a P-11 Pion-Nucleon Resonance at 556 MeV. *Phys. Rev. Lett.*, 12:340–342, 1964.
 - [2] N. Suzuki, B. Juliá-Díaz, H. Kamano, T.-S. H. Lee, A. Matsuyama, and T. Sato. Disentangling the Dynamical Origin of P 11 Nucleon Resonances. *Physical Review Letters*, 104(4):042302, 2010.
 - [3] Zhan-Wei Liu, Waseem Kamleh, Derek B. Leinweber, Finn M. Stokes, Anthony W. Thomas, and Jia-Jun Wu. Hamiltonian ef-

fective field theory study of the $N^*(1440)$ resonance in lattice QCD. *Phys. Rev. D*, 95(3):034034, 2017.

- [4] Si-xue Qin, Craig D Roberts, and Sebastian M Schmidt. Spectrum of light- and heavy-baryons. *Few Body Syst.*, 60(2):26, 2019.
- [5] Jia-jun Wu, Derek B. Leinweber, Zhan-wei Liu, and Anthony W. Thomas. Structure of the Roper Resonance from Lattice QCD Constraints. *Phys. Rev. D*, 97(9):094509, 2018.

- [6] C. B. Lang, L. Leskovec, M. Padmanath, and S. Prelovsek. Pion-nucleon scattering in the Roper channel from lattice QCD. *Phys. Rev. D*, 95(1):014510, 2017.
- [7] Daiki Suenaga and Atsushi Hosaka. Decays of Roper-like singly heavy baryons in a chiral model. *Phys. Rev. D*, 105(7):074036, 2022.
- [8] H. Clement, T. Skorodko, and E. Doroshkevich. Possibility of dibaryon formation near the $N^*(1440)N$ threshold: Reexamination of isoscalar single-pion production. *Phys. Rev. C*, 106(6):065204, 2022.
- [9] James S. Ball, Gordon L. Shaw, and David Y. Wong. Two-Channel Model of P-11pi-N Partial-Wave Amplitude. *Phys. Rev.*, 155:1725–1727, 1967.
- [10] Bing-Song Zou. Roper resonance $N^*(1440)$ from charmonium decays. 9 2025.
- [11] Qiang Zhao and Frank E. Close. Quarks, diquarks and QCD mixing in the N^* resonance spectrum. *Phys. Rev. D*, 74:094014, 2006.
- [12] Bingwei Long and U. van Kolck. The Role of the Roper in Chiral Perturbation Theory. *Nucl. Phys. A*, 870-871:72–82, 2011.
- [13] Chen Chen, Bruno El-Bennich, Craig D. Roberts, Sebastian M. Schmidt, Jorge Segovia, and Shaolong Wan. Structure of the nucleon’s low-lying excitations. *Phys. Rev. D*, 97(3):034016, 2018.
- [14] Yue Tan, Zi-Xuan Ma, Xiaoyun Chen, Xiaohuang Hu, Youchang Yang, Qi Huang, and Jialun Ping. Investigating the nature of $N(1535)$ and $\Lambda(1405)$ in a quenched chiral quark model. *Phys. Rev. D*, 111(9):096018, 2025.
- [15] Peng Cheng, Langtian Liu, Ya Lu, and Craig D. Roberts. Insights into Nucleon Resonances via Continuum Schwinger Function Methods. 12 2025.
- [16] S. Godfrey and Nathan Isgur. Mesons in a Relativized Quark Model with Chromodynamics. *Phys. Rev. D*, 32:189–231, 1985.
- [17] Simon Capstick and Nathan Isgur. Baryons in a relativized quark model with chromodynamics. *Phys. Rev. D*, 34(9):2809–2835, 1986.
- [18] L. Ya. Glozman and D. O. Riska. The Spectrum of the nucleons and the strange hyperons and chiral dynamics. *Phys. Rept.*, 268:263–303, 1996.
- [19] Hui-Hua Zhong, Ming-Sheng Liu, Ru-Hui Ni, Mu-Yang Chen, Xian-Hui Zhong, and Qiang Zhao. Unified study of nucleon and Δ baryon spectra and their strong decays with chiral dynamics. *Phys. Rev. D*, 110:116034, Dec 2024.
- [20] B. Julia-Diaz and D. O. Riska. The Role of qqqq anti-q components in the nucleon and the $N(1440)$ resonance. *Nucl. Phys. A*, 780:175–186, 2006.
- [21] S. Navas et al. Review of particle physics. *Phys. Rev. D*, 110(3):030001, 2024.
- [22] R. Bijker, J. Ferretti, G. Galatà, H. García-Tecocoatzi, and E. Santopinto. Strong decays of baryons and missing resonances. *Phys. Rev. D*, 94(7):074040, 2016.
- [23] B. C. Hunt and D. M. Manley. Updated determination of N^* resonance parameters using a unitary, multichannel formalism. *Phys. Rev. C*, 99(5):055205, 2019.
- [24] Jambul Gegelia, Ulf-G. Meißner, and De-Liang Yao. The width of the Roper resonance in baryon chiral perturbation theory. *Phys. Lett. B*, 760:736–741, 2016.
- [25] Volker D. Burkert and Craig D. Roberts. Colloquium : Roper resonance: Toward a solution to the fifty year puzzle. *Rev. Mod. Phys.*, 91(1):011003, 2019.
- [26] V. Shklyar, H. Lenske, and U. Mosel. η -meson production in the resonance-energy region. *Phys. Rev. C*, 87(1):015201, 2013.
- [27] Martin Hoferichter, Jacobo Ruiz de Elvira, Bastian Kubis, and Ulf-G. Meißner. Nucleon resonance parameters from Roy–Steiner equations. *Phys. Lett. B*, 853:138698, 2024.
- [28] Deborah Rönchen, Michael Döring, Ulf-G. Meißner, and Chao-Wei Shen. Light baryon resonances from a coupled-channel study including $K\Sigma$ photoproduction. *Eur. Phys. J. A*, 58(11):229, 2022.
- [29] A. V. Anisovich, R. Beck, E. Klempt, V. A. Nikonov, A. V. Sarantsev, and U. Thoma. Properties of baryon resonances from a multichannel partial wave analysis. *Eur. Phys. J. A*, 48:15, 2012.
- [30] R. A. Arndt, W. J. Briscoe, I. I. Strakovsky, and R. L. Workman. Extended partial-wave analysis of piN scattering data. *Phys. Rev. C*, 74:045205, 2006.
- [31] B. C. Pearce and B. K. Jennings. A Relativistic meson exchange model of pion - nucleon scattering. *Nucl. Phys. A*, 528:655–675, 1991.
- [32] Yu-Fei Wang, Ulf-G. Meißner, Deborah Rönchen, and Chao-Wei Shen. Examination of the nature of the N^* and Δ resonances via coupled-channels dynamics. *Physical Review C*, 109(1):015202, January 2024.
- [33] O. Krehl, C. Hanhart, S. Krewald, and J. Speth. What is the structure of the Roper resonance? *Physical Review C*, 62(2):025207, 2000.
- [34] Li-Ye Xiao, Xu Cao, and Xian-Hui Zhong. Neutral pion photoproduction on the nucleon in a chiral quark model. *Phys. Rev. C*, 92(3):035202, 2015.
- [35] Zhiguang Xiao and Zhi-Yong Zhou. Partial Wave Decomposition in Friedrichs Model With Self-interacting Continua. *J. Math. Phys.*, 58:072102, 2017.
- [36] Zhiguang Xiao and Zhi-Yong Zhou. Virtual states and the generalized completeness relation in the Friedrichs model. *Physical Review D*, 94(7):076006, October 2016.
- [37] Zhiguang Xiao and Zhi-Yong Zhou. On the generalized Friedrichs-Lee model with multiple discrete and continuous states*. *Chin. Phys.*, 49(8):083102, 2025.
- [38] O. Civitarese and M. Gadella. Physical and mathematical aspects of gamow states. *Communications on Pure and Applied Mathematics*, 396(2):41–113, 2004.
- [39] T. D. Lee. Some Special Examples in Renormalizable Field Theory. *Phys. Rev.*, 95:1329–1334, 1954.
- [40] K. O. Friedrichs. On the perturbation of continuous spectra. *Commun. Pure Appl. Math.*, 1(4):361–406, 1948.
- [41] Nathan Isgur and Gabriel Karl. P Wave Baryons in the Quark Model. *Phys. Rev. D*, 18:4187, 1978.
- [42] Nathan Isgur and Gabriel Karl. Positive Parity Excited Baryons in a Quark Model with Hyperfine Interactions. *Phys. Rev. D*, 19:2653, 1979.
- [43] R. K. Bhaduri, L. E. Cohler, and Y. Nogami. A unified potential for mesons and baryons. *Il Nuovo Cimento A (1965-1970)*, 65(3):376–390, 1981.
- [44] C. S. Kalman and B. Tran. Baryon spectrum in a potential quark model. 102(3):835–879.
- [45] Ming-Sheng Liu, Kai-Lei Wang, Qi-Fang Lü, and Xian-Hui Zhong. Ω baryon spectrum and their decays in a constituent quark model. *Phys. Rev. D*, 101(1):016002, 2020.
- [46] Muslema Pervin and Winston Roberts. Strangeness -2 and -3 baryons in a constituent quark model. *Phys. Rev. C*, 77:025202, 2008.
- [47] W. Roberts and Muslema Pervin. Heavy baryons in a quark model. *Int. J. Mod. Phys. A*, 23:2817–2860, 2008.
- [48] E. Hiyama, Y. Kino, and M. Kamimura. Gaussian expansion method for few-body systems. *Prog. Part. Nucl. Phys.*, 51:223–307, 2003.
- [49] L. Micu. Decay rates of meson resonances in a quark model.

- Nucl. Phys. B*, 10:521–526, 1969.
- [50] Robert D. Carlitz and M. Kislinger. Regge amplitude arising from $su(6)_w$ vertices. *Phys. Rev. D*, 2:336–342, 1970.
- [51] A. Le Yaouanc, L. Oliver, O. Pene, and J. C. Raynal. Naive quark pair creation model of strong interaction vertices. *Phys. Rev. D*, 8:2223–2234, 1973.
- [52] Zhi-Yong Zhou and Zhiguang Xiao. Understanding $X(3862)$, $X(3872)$, and $X(3930)$ in a Friedrichs-model-like scheme. *Phys. Rev. D*, 96(5):054031, 2017. [Erratum: *Phys.Rev.D* 96, 099905 (2017)].
- [53] Steven Weinberg. Elementary particle theory of composite particles. *Phys. Rev.*, 130:776–783, 1963.
- [54] Tetsuo Hyodo. Structure and compositeness of hadron resonances. *Int. J. Mod. Phys. A*, 28:1330045, 2013.
- [55] Takayasu Sekihara, Tetsuo Hyodo, and Daisuke Jido. Comprehensive analysis of the wave function of a hadronic resonance and its compositeness. *PTEP*, 2015:063D04, 2015.
- [56] Tomona Kinugawa and Tetsuo Hyodo. Compositeness of hadrons, nuclei, and atomic systems. *Eur. Phys. J. A*, 61(7):154, 2025.
- [57] Zhi-Hui Guo and J. A. Oller. Probabilistic interpretation of compositeness relation for resonances. *Phys. Rev. D*, 93(9):096001, 2016.
- [58] F. Aceti, L. R. Dai, L. S. Geng, E. Oset, and Y. Zhang. Meson-baryon components in the states of the baryon decuplet. *Eur. Phys. J. A*, 50:57, 2014.
- [59] Yuki Kamiya and Tetsuo Hyodo. Structure of near-threshold quasibound states. *Phys. Rev. C*, 93(3):035203, 2016.
- [60] Yuki Kamiya and Tetsuo Hyodo. Generalized weak-binding relations of compositeness in effective field theory. *PTEP*, 2017(2):023D02, 2017.
- [61] V. I. Mokeev and D. S. Carman. Roper Resonance Structure and Exploration of Emergent Hadron Mass from CLAS Electroproduction Data. 11 2025.
- [62] Daisuke Jido Tetsuo Hyodo and Atsushi Hosaka. Origin of resonances in the chiral unitary approach. *Prog. Part. Nucl. Phys.*, 2008.
- [63] Norbert Kaiser, P. B. Siegel, and W. Weise. Chiral dynamics and the $S_{11}(1535)$ nucleon resonance. *Phys. Lett. B*, 362:23–28, 1995.
- [64] J. Nieves and E. Ruiz Arriola. The $S(11) - N(1535)$ and $-N(1650)$ resonances in meson baryon unitarized coupled channel chiral perturbation theory. *Phys. Rev. D*, 64:116008, 2001.
- [65] Peter C. Bruns, Maxim Mai, and Ulf G. Meissner. Chiral dynamics of the $S_{11}(1535)$ and $S_{11}(1650)$ resonances revisited. *Phys. Lett. B*, 697:254–259, 2011.
- [66] M. Doring and K. Nakayama. The Phase and pole structure of the $N^*(1535)$ in $\pi N \rightarrow \pi N$ and $\gamma N \rightarrow \pi N$. *Eur. Phys. J. A*, 43:83–105, 2010.
- [67] Zhan-Wei Liu, Waseem Kamleh, Derek B. Leinweber, Finn M. Stokes, Anthony W. Thomas, and Jia-Jun Wu. Hamiltonian effective field theory study of the $N^*(1535)$ resonance in lattice QCD. *Phys. Rev. Lett.*, 116(8):082004, 2016.
- [68] Jun He, B. Saghai, and Zhenping Li. Study of η photoproduction on the proton in a chiral constituent quark approach via one-gluon-exchange model. *Phys. Rev. C*, 78:035204, 2008.
- [69] Xian-Hui Zhong and Qiang Zhao. η photoproduction on the quasi-free nucleons in the chiral quark model. *Phys. Rev. C*, 84:045207, 2011.
- [70] Zhi-Yong Zhou and Zhiguang Xiao. Two-pole structures in a relativistic Friedrichs–Lee-QPC scheme. *Eur. Phys. J. C*, 81(6):551, 2021.
- [71] E. J. Garzon, J. J. Xie, and E. Oset. Case in favor of the $N^*(1700)(3/2^-)$. *Phys. Rev. C*, 87(5):055204, 2013.